EVOLUTION OF THE ATOMIC STRUCTURE OF CADMIUM IN THE HEATING AND COOLING PROCESS

Sedat Sengul[1], Murat Celtek[2], Unal Domekeli[1]

[1]*Dept. of Physics, Trakya University, 22030, Edirne – TURKEY*
[2]*Faculty of Education, Trakya University, 22030, Edirne – TURKEY*

Abstract

The atomic structure of solid and liquid cadmium was investigated by molecular dynamics simulations using the tight-binding many-body potentials. Four different cooling rates (10, 2, 0.2 and 0.02 K/ps) were chosen to investigate the effect of cooling rate in the rapid solidification process. In order to monitor the structural evolution of the system during the cooling processes, methods such as pair distribution function, structure factor, Honeycutt-Andersen bond type index analysis etc. were used. The melting point of hcp cadmium was found to be 560±10 K, which is in agreement with the experimental melting point of 594.3 K. It was observed that there is a good agreement between the experimental results reported in the literature for liquid cadmium and the total pair distribution function and structure factors we calculated. A first-order phase transition is not observed for rapidly cooled (10 and 2 K/ps) liquid cadmium, whereas a liquid-solid phase transition is observed for slower cooling rates (0.2 and 0.02 K/ps). According to the results of the Honeycutt-Andersen analysis, 1431, 1541 and 1551 bonded pairs, which indicate the existence and development of icosahedral order, are dominant in rapidly cooled systems, while 1421 bonded pairs, which represent fcc-like crystalline structures, dominate in slower cooling systems. It has been observed that the tight-binding many-body potential accurately predicts the physical properties of cadmium at both low and high temperatures.

Keywords: Cadmium, Molecular Dynamics Simulations, Tight-binding potential, Structure factor, Honeycutt-Andersen analysis

INTRODUCTION

A hexagonal closed packed (hcp) cadmium (Cd) element with a low melting point (594.3 K [1]) has great importance due to its use in many fields. It is found in nature mostly in the form of cadmium sulfide (CdS) or among zinc ores. Cd is almost the only substance that gives the yellow color to paint, soap, textile, and paper. Cadmium sulfate is used as a mild antiseptic in medicine. Moreover, accumulators with Cd electrodes have a longer life than lead batteries. Cadmium bromide and cadmium iodide give silver nitrate collodion plates in photography the iodide necessary for the formation of silver iodide. Moreover, as a pure metal, Cd is an essential material for the construction of control rods in nuclear reactors. It is used as a coating on steel, iron, copper and zinc as it provides resistance to corrosion. Since Cd crystallizes in the hcp structure with an unusually large c/a axial ratio, there are many theoretical and experimental studies on it in the literature [2–4]. This anomaly is observed in solid zinc, where an electronic topological transition usually occurs at high pressures, and this is still a matter of open debate [2]. These unique properties of the element Cd motivated us to further research it. Thus, we focused on the heating and cooling process of Cd. To investigate the effect of cooling rate on Cd microstructure, the system has been cooled with four different cooling rates (γ_1=10, γ_2=2, γ_3=0.2 and γ_4=0.02 K/ps). In these processes, the structural evolution of Cd has been followed by the classical molecular dynamics (MD) simulation method. In simulations, the tight binding (TB) many-body potential which is widely preferred for metallic systems in the literature, is employed to express interactions between Cd atoms [5]. We used the OVITO program to monitor and analyze atomic simulation results [6].

EXPOSITION

In the TB second-moment approximation (SMA), the band energy of the system is

proportional to the square root of the second moment of the state density. The assumptions underlying this approach have been reviewed by Cleri and Rosato [5]. The form of the potential energy (U_s) is given as [7–9]:

$$U_s = \sum_i \left(E_i^R + E_i^B\right), \quad (1)$$

where E_i^R and E_i^B represent a repulsive potential and cohesive band energy term, respectively.

$$E_i^R = \sum_{j \neq i} U_{ij}(r_{ij}), \quad (2)$$

$$U_{ij}(r_{ij}) = A \exp\left[-p\left(\frac{r_{ij}}{r_0} - 1\right)\right] \quad (3)$$

$$E_i^B = \left(\sum_{j \neq i} \phi_{ij}(r_{ij}),\right)^{1/2} \quad (4)$$

$$\phi_{ij}(r_{ij}) = \xi^2 \exp\left[-2q\left(\frac{r_{ij}}{r_0} - 1\right)\right] \quad (5)$$

The values of TB potential parameters for Cd are listed in Table 1.

Table 1. TB potential parameters for the Cd [5].

	ξ (eV)	A (eV)	q	p	r_0 (Å)
Cd	0.4720	0.0416	3.9080	13.6390	2.9800

All MD simulations were performed with the DLPOLY software, general-purpose atomic simulation package developed by Smith and his work group [10]. The simulations were performed in a box with 12960 Cd atoms under three-dimensional periodic boundary conditions. The Berendsen thermostat and barostat were used to control temperature and pressure, respectively. The leapfrog Verlet algorithm with a time step of 1 fs (or 0.001 ps) was used to solve the equations of motion. The initial configuration was created by placing the positions of the Cd atoms in the unit cell in accordance with the hcp crystalline arrangement. The isothermal-isobaric (NPT) ensemble (constant number of atoms, pressure, and temperature) was used throughout the heating and cooling process. First, the system was heated with an interval of 50 K from 0 K to 700 K. Then, the liquid system, which was equilibrated by annealing at 700 K, was cooled down to 50 K with four different cooling rates (γ_1=10, γ_2=2, γ_3=0.2 and γ_4=0.02 K/ps). In order to determine the melting point more precisely, the region where the first-order phase transition was observed was studied at 10 K intervals. The volume-temperature (V-T) curves obtained during the heating and cooling processes are shown in Figure 1. As expected, the volume of the heated system increases, and there is a sharp increase in the V-T curve around 560 K, representing the solid-liquid phase transition. The calculated melting temperature T_m^{MD} = 560 K shows good agreement with the experimental melting temperature T_m^{exp} = 594.3 K [1], considering the differences between MD simulations and experimental conditions. Interestingly, at lower temperatures (around 200-250 K), there is an unexpected decrease in volume, but it is difficult to conclude whether it is a solid-solid phase transition. This observation will be discussed in the following sections with different analysis methods. We will consider the cooling process under two main headings; the first is the liquid-amorphous transformation, and the second is the liquid-crystal phase transition. The volume decreases almost linearly up to around 350 K for all cooling rates and they are each close to each other. For cooling rates of γ_1=10 and γ_2=2 K/ps, the V-T curve changes smoothly after vitrification, whereas for cooling rates of γ_3=0.2 and γ_4=0.02 K/ps, a sudden change in V-T over a narrow temperature range indicates a crystallization event. From these findings, it can be seen that the phase formation during the cooling process is highly dependent on the cooling rates.

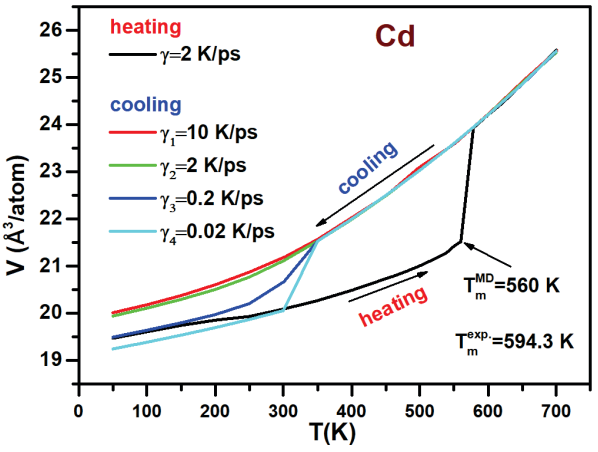

Fig. 1. *Change of volume as a function of temperature during heating and cooling processes.*

The pair distribution function (PDF or g(r)) has been used to characterize the atomic structure through both processes. It also provides useful information for us to follow and interpret phase transitions. Thus, the total g(r) is defined as [11]

$$g(r) = \frac{\Omega}{N^2}\left\langle \sum_{i}^{N}\sum_{i\neq j}^{N} \delta(r - r_{ij}) \right\rangle, \qquad (6)$$

where N and Ω represent the total number of atoms in the simulation box and its volume, respectively. The calculated g(r) and structure factor (SF or S(q)) for liquid Cd at 620 K are shown in Figure 2 together with the experimental results (623 K) [12]. As can be seen from the figure, there is a perfect agreement between the g(r) and S(q) curves we calculated from the TB-MD simulations and their experimental data. This is proof that the TB potential we selected can successfully explain the structural properties of liquid Cd.

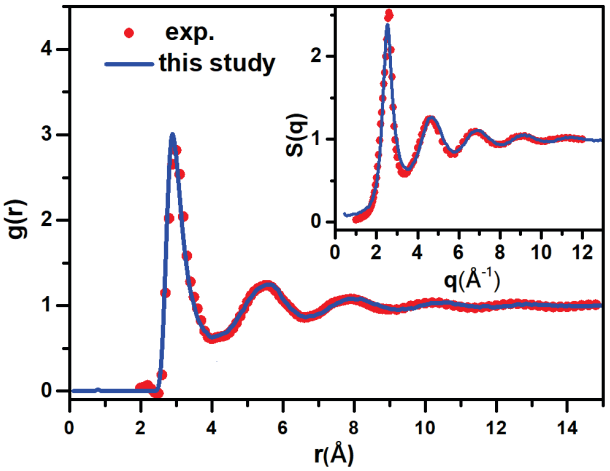

Fig. 2. *Comparison of calculated (620 K) and experimental (623 K) g(r) and S(q) curves for liquid Cd.*

Figure 3 presents a comparison of the g(r)'s calculated at different temperatures with the cooling rates of γ_2=2 and γ_4=0.02 K/ps, and the g(r)'s calculated during the heating process. In order to avoid repetition and visual pollution, the results obtained for other cooling rates are not included in this figure. The main peaks of the g(r) curves calculated during the heating process exhibit peak behavior specific to crystalline structures. These are narrow and high peaks. With increasing temperature, the heights of these peaks decrease and their widths increase. And finally, when the temperature is increased by 600 K, some of these peaks disappear and the visible peaks exhibit a behavior specific to liquid structures, that is, they now have much wider and lower heights. This is also a sign that the system is melting. The g(r) curves calculated for the heating and cooling processes at 600 K and 700 K overlap, indicating that there is enough free space in the system for the atoms to move. At 400 K and 500 K, the g(r) curves calculated for both cooling rates overlap, while the curves obtained from heating produce peaks specific to crystal-like structures. When the temperature is lowered further, the g(r) curves obtained from two different cooling rates at 300 K and 200 K exhibit very different behavior from each other. The g(r)'s calculated for the cooling rate of γ_2=2 K/ps are similar to those of liquid systems, but unlike them, a splitting occurs at the second maximum peaks, which indicates the development of medium-range order and is characteristic of amorphous structures. However, there are differences in the positions and heights of the peaks of g(r) obtained in the heating and cooling processes towards larger r values, which may be due to the proportionality of atoms with different hcp and fcc orders in both processes.

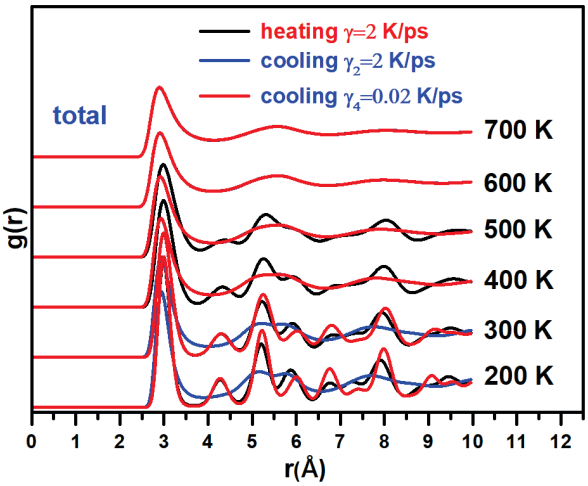

Fig. 3. *g(r) curves calculated at different temperatures during heating (γ=2 K/ps) and cooling (γ_2=2 and γ_4=0.02 K/ps) processes.*

There are many methods in the literature to determine the glass transition temperature (T_g) and crystallization temperature (T_c). Among them, one of the analysis methods that gives the simplest and most accurate results is the Wendt-Abraham parameter ($R^{WA}=g_{min}/g_{max}$) [13]. Recently, Celtek et al. performed a minor modification on the R^{WA} correlation and defined the new correlation as ($R^{MWA}=(g_{min}/g_{max})^2$) [8, 14]. Here g_{min} and g_{max} are the first minimum and maximum of g(r), respectively. As an example, the temperature-

dependent evolution of the R^{MWA} parameter calculated for a cooling rate of γ_2=2 K/ps is shown in Figure 4. We determined the intersection point of the fit curves drawn separately for the low and high-temperature regions as T_g. The results of the fit procedure are given embedded in the inset of the figure for both regions. According to the R^{MWA} parameter, T_g's for γ_1=10 and γ_2=2 K/ps have been determined as ~360 K and ~340 K, respectively, and T_c's for γ_3=0.2 and γ_4=0.02 K/ps have been determined as ~250 K and ~300 K, respectively.

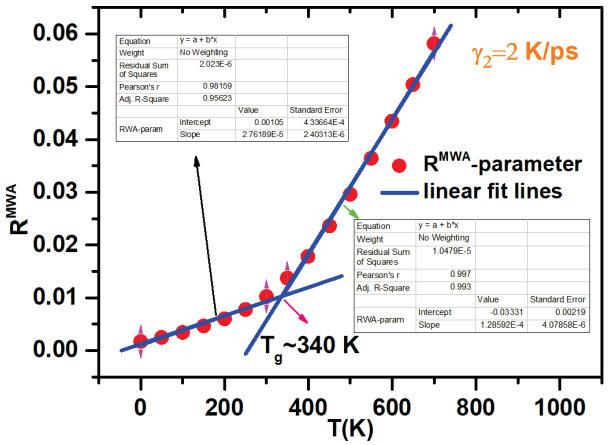

Fig. 4. *Evolution of the R^{MWA} parameter as a function of temperature for a cooling rate of γ_2=2 K/ps.*

The evolution of the topological arrangement of the system during the cooling or heating processes is analyzed using the Honeycutt-Andersen (HA) bond type index, which provides analysis based on the atomic pairs and the atomic arrangement around them [15, 16]. In the HA method, a sequence of four indices such as *ijkl* is used to characterize the local environment of the pair. For example, the only bonded pair in the fcc crystal is 1421, while the hcp crystal has the numbers 1422 and 1421. The 1661 and 1441 bonded pairs are related to a bcc crystal. The 1551 bonded pair is characteristic of the icosahedral order, while the 1431 and 1541 are characteristic of the defective icosahedral structure [17, 18].

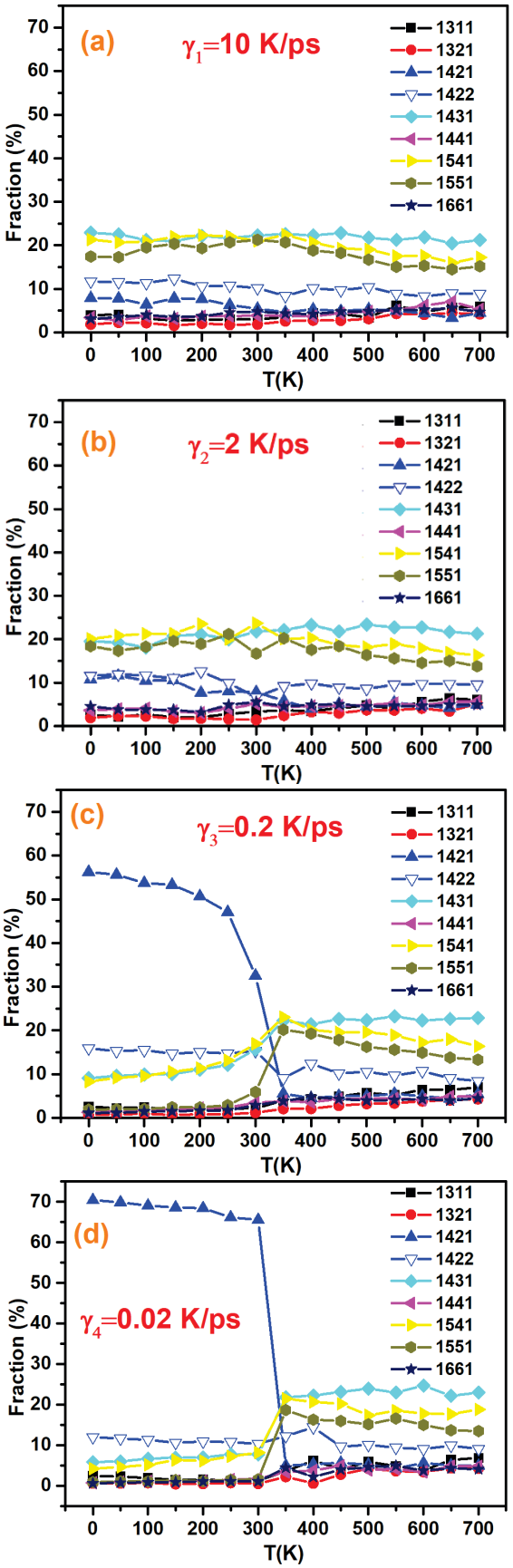

Fig. 5. *Fraction of the most popular HA bonded pairs calculated for cooling rates of (a) γ_1=10 K/ps, (b) γ_2=2 K/ps, (c) γ_3=0.2 K/ps and (d) γ_4=0.02 K/ps.*

The temperature-dependent evolution of the nine most common bonded pairs for the four cooling rates is shown in Figure 5 (a-d). The results for cooling rates of γ_1=10 and γ_2=2 K/ps show that the majority of pairs at all temperatures are 1551, 1541 and 1431 bonded pairs, indicating that icosahedral packing dominates due to more favorable energy [19]. This indicates that the short-range order has developed in the system and that the system has changed from a liquid to an amorphous state. For lower temperatures, they are followed by 1422 and 1421 bonded pairs representing the hcp/fcc crystal. Consistent with the above results for these cooling rates, no change is observed to indicate a first-order phase transition. As can be seen in Figures 5(c) and 5(d), the results of cooling rates of γ_3=0.2 and γ_4=0.02 K/ps show different behavior compared to the results of other cooling rates. At high temperatures, while the fraction of pairs representing ideal icosahedral and defective icosahedral order is high, a sudden decrease in their fraction and a very sharp increase in 1421 bonded pairs representing fcc crystal order are observed around 350 K. This abrupt change in the bonded pairs indicates that the more slowly cooled system makes a liquid-crystalline phase transition at these temperature points. 1421 bonded pairs are followed by 1422 bonded pairs. For a cooling rate of γ_3=0.2 K/ps, the fraction of 1421 (or 1422) bonded pairs increases to around ~55% (or ~17%) at 50 K, while this ratio rises to around ~70% (or ~12%) for γ_4=0.02 K/ps. This shows us that in the formation of the crystal order of the system in the slow cooling process, the hcp and fcc crystal structures are in a race, and in the system that is cooled more slowly, the pairs representing the fcc structure dominate compared to the other pairs. To support these results with visual data, we have shown the fcc and hcp atom distributions in the simulation boxes in the heating and cooling (only for cooling rates of γ_3=0.2 and γ_4=0.02 K/ps) processes at 300K together in Figure 6. While the number of atoms with hcp crystal order is high during the heating process, it is seen that atoms with a certain amount of fcc order begin to form between them. Findings from the cooling rate of γ_3=0.2 K/ps show that the atomic distributions with hcp and fcc crystalline order are in a random manner and the number of atoms with fcc crystalline order is higher. The snapshots taken for the system cooled with γ_4=0.02 K/ps cooling rate are quite different and interesting from the others. From the snapshots, it is seen that the hcp and fcc atoms in the upper and lower regions of the simulation box are separated into layers, while interestingly, the middle region of the box is completely filled by atoms with fcc crystalline order. All these findings are consistent with the results discussed above.

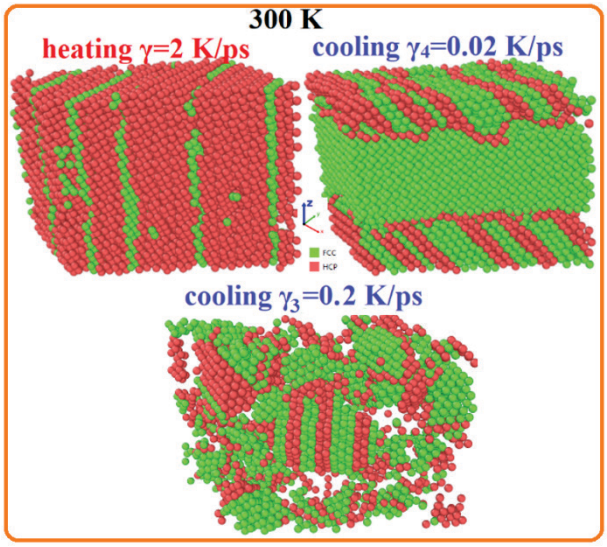

Fig. 6. *Snapshots of the simulation box obtained for the heating and cooling (γ_3=0.2 and γ_4=0.02 K/ps) processes at 300K.*

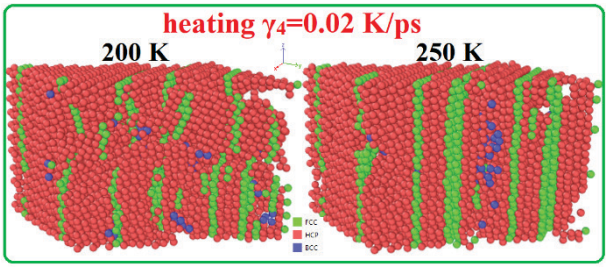

Fig. 7. *Snapshots showing the crystalline order in the simulation box during the heating process at 200 K and 250 K.*

There is no evidence that the small change observed in the 200-250 K regions of the V-T curve obtained for the heating process in Figure 1 is a solid-solid phase transition. However, to present a different perspective, we present the maternity images showing the crystal arrangement at 200 K and 250 K in Figure 7. As can be seen from the snapshots, a noticeable increase is observed in the number of atoms with fcc crystalline order when the temperature

is increased to 250K. The increase in the number of atoms with fcc order may be the reason for the small volume change that has been mentioned.

CONCLUSION

The evolution of the microstructure of the hcp crystalline Cd during the heating and cooling processes was investigated by MD simulations using the TB-SMA potential. The results show that the TB-SMA potential accurately predicts the melting point of solid Cd and the calculated g(r) and S(q) for liquid Cd are in excellent agreement with the experimental results. While no evidence of first-order phase transition has been observed for the rapidly cooled (γ_1=10 and γ_2=2 K/ps) liquid Cd, the liquid-solid phase transition has been observed for the more slowly cooled (γ_3=0.2 and γ_4=0.02 K/ps) system. For cooling rates of γ_1=10 and γ_2=2 K/ps, 1551, 1541 and 1431 bonded pairs representing icosahedral and defective icosahedral order were dominant at all temperatures, while for other cooling rates, 1421 and 1422 bonded pairs were dominant at lower temperatures. For the systems cooled slowly, T_g values decreased while Tc values increased. Interestingly, Cd with hcp crystalline order exhibited a distribution suitable for fcc crystalline order when cooled with a cooling rate of γ_4=0.02 K/ps. We believe that the results will contribute to the understanding of the behavior of Cd during the cooling and heating process.

REFERENCE

[1] Kittel C. Introduction to Solid State Physics. New York: John Wiley & Sons Inc., 1986.

[2] Minicucci M, Trapananti A, Cicco A Di, et al. Cadmium under High Pressure and High Temperature Conditions. Phys Scr 2005; 1056.

[3] Lai SK, Li W, Tosi MP. Evaluation of liquid structure for potassium, zinc, and cadmium. Phys Rev A 1990; 42: 7289–7303.

[4] Kenichi T. Structural study of Zn and Cd to ultrahigh pressures. Phys Rev B 1997; 56: 5170–5179.

[5] Cleri F, Rosato V. Tight-binding potentials for transition metals and alloys. Phys Rev B 1993; 48: 22–33.

[6] Stukowski A. Visualization and analysis of atomistic simulation data with OVITO-the Open Visualization Tool. Model Simul Mater Sci Eng 2010; 18: 015012.

[7] Senturk Dalgic S, Celtek M. Liquid -to-glass transition in bulk glass-forming Cu55-xZr45Agx alloys using molecular dynamic simulations. EPJ Web Conf 2011; 15: 03009.

[8] Celtek M, Sengul S, Domekeli U, et al. Dynamical and structural properties of metallic liquid and glass Zr48Cu36Ag8Al8 alloy studied by molecular dynamics simulation. J Non Cryst Solids 2021; 566: 120890.

[9] Sengul S, Celtek M, Domekeli U. Molecular dynamics simulations of glass formation and atomic structures in Zr60Cu20Fe20 ternary bulk metallic alloy. Vacuum 2017; 136: 20–27.

[10] Smith W, Forester TR. DL_POLY_2.0: A general-purpose parallel molecular dynamics simulation package. J Mol Graph 1996; 14: 136–141.

[11] Celik FA. Molecular dynamics simulation of polyhedron analysis of Cu–Ag alloy under rapid quenching conditions. Phys Lett A 2014; 378: 2151–2156.

[12] Waseda Y. The Structure of Non-Crystalline Materials-Liquids and Amorphous Solids. New York: London: McGraw-Hill, 1981.

[13] Wendt HR, Abraham FF. Empirical Criterion for the Glass Transition Region Based on Monte Carlo Simulations. Phys Rev Lett 1978; 41: 1244–1246.

[14] Celtek M. Atomic structure of Cu60Ti20Zr20 metallic glass under high pressures. Intermetallics 2022; 143: 107493.

[15] Celtek M, Domekeli U, Sengul S, et al. Effects of Ag or Al addition to CuZr-based metallic alloys on glass formation and structural evolution: a molecular dynamics simulation study. Intermetallics 2021; 128: 107023.

[16] Honeycutt JD, Andersen HC. Molecular Dynamics Study of Melting and Freezing of Small Lennard- Jones Clusters. J Phys Chem 1987; 91: 4950–4963.

[17] Guder V, Sengul S, Celtek M, et al. Pressure dependent evolution of microstructures in Pd80Si20 bulk metallic glass. J Non Cryst Solids 2022; 576: 121290.

[18] Celtek M. An in-depth investigation of the microstructural evolution and dynamic properties of Zr77Rh23 metallic liquids and glasses: A molecular dynamics simulation study. J Appl Phys 2022; 132: 035902.

[19] Sun YL, Shen J, Valladares AA. Atomic structure and diffusion in Cu60Zr40 metallic liquid and glass: molecular dynamics simulations. J Appl Phys 2009; 106: 073520.